Why is the Pacific Meridional Mode Most Pronounced in Boreal Spring?

Zilu Meng[1], Tim Li[2,1]

[1] Key Laboratory of Meteorological Disaster, Ministry of Education (KLME) / Joint International Research Laboratory of Climate and Environmental Change (ILCEC) / Collaborative Innovation Center on Forecast and Evaluation of Meteorological Disasters (CIC-FEMD), Nanjing University of Information Science and Technology, Nanjing, China

[2] Department of Atmospheric Sciences, University of Hawai'i at Manoa, Honolulu, Hawaii, USA

Corresponding author: Tim Li (timli@hawaii.edu)

†Department of Atmospheric Sciences, University of Hawai'i at Manoa, Honolulu, Hawaii

Key Points:

- The Pacific Meridional Mode is strongest in boreal spring results from the impact of the mean trade wind in latent heat flux anomaly.
- Simple coupled model experiments demonstrated that the greatest strength and area of the northeasterly trade is the main reason.

Abstract

The Pacific Meridional Mode (PMM) exhibits a marked seasonal variability, with the strongest (weakest) variance in northern spring (fall). Such a phase locking feature is investigated through a combined observational and modeling study. Given the PMM perturbation, the wind induced latent heat flux anomaly leads to a strongest (weakest) heating on local sea surface temperature anomaly (SSTA) in MAM (SON) through positive wind-evaporation-SST feedback. The difference between MAM and SON lies on the strength and area of mean northeasterly trades. Experiments with a simple air-sea coupled model further demonstrate that a PMM-like SSTA perturbation grows much faster in MAM than in SON. The difference is primarily attributed to the seasonal mean wind, not mean SST condition. It is greatest strength and area of the mean northeasterly trade in MAM that leads to most efficient wind-evaporation-SST feedback and thus fastest PMM growth rate.

Plain Language Summary

The Pacific Meridional Mode (PMM) is an important climate mode and may influence the development of El Nino. PMM exhibits a great seasonality, with strongest (weakest) intensity in boreal spring (fall). The cause of this season-dependence is investigated through both observational analyses and idealized coupled model experiments. It is found that given the fixed observed PMM related anomalous wind field, the surface latent heat flux anomaly that heats the ocean surface is greatest (weakest) under the boreal spring (autumn) mean condition. A simple coupled atmosphere-ocean model is further used to estimate the growth rate of the PMM under different seasonal mean wind and SST conditions. It is found that the seasonal mean wind plays a dominant role. The greatest strength and area of the mean northeasterly trade in MAM favors most efficient wind-evaporation-SST feedback and thus fastest PMM growth.

1 Introduction

A marked sea surface temperature anomaly (SSTA) pattern in the tropical Pacific, in addition to the El Niño pattern, is the Pacific Meridional Mode (PMM) (Chiang & Vimont, 2004). The PMM is characterized by a northeast-southwest tilted SSTA structure, extending from Baja California all the way to central-western equatorial Pacific. Accompanied with a positive PMM-like SSTA pattern are pronounced low-level southwesterly anomalies in situ, implying a positive wind-evaporation-SST (WES) feedback (Xie & Philander, 1994; Li & Philander, 1996). As a precursor signal, the PMM might gradually evolve to an ENSO event (Alexander et al., 2010).

Due to the WES feedback, the PMM may be triggered by perturbations from tropics or mid-latitudes. A typical source of the mid-latitude forcing is the North Pacific Oscillation (NPO) (Vimont et al., 2009). The main mechanism for the development and maintenance of the PMM involves the wind-evaporation-SST feedback (Vimont et al. 2009; Wu et al. 2009). In response to a positive SSTA forcing, a low-level cyclonic wind anomaly is generated to the west of the anomalous heat source, as a Rossby wave response (Gill, 1980). Southwesterly surface wind anomalies associated with the cyclone overlap the warm SSTA, leading to reduced surface evaporation as the mean wind is northeasterly in the region. The reduced surface evaporation or latent heat flux amplifies the warm SSTA in situ, leading to the growth of the PMM.

It has been shown that the PMM may exert a great impact on ENSO development (e.g., Amaya 2019). So far two mechanisms have been proposed. The first is the seasonal foot-printing mechanism (SFM) (Vimont et al. 2003; Alexander et al. 2010). The other is so called summer deep convective heating (SDC) mechanism (Amaya et al., 2019). Because of their close link, the PMM is taken as a predictor for ENSO prediction (e.g., Zhang et al. 2009; Lorenzo et al. 2015; Stuecker 2018).

It is worth noting that while the PMM pattern may occur in all seasons, its peak phase happens in boreal spring (Alexander et al., 2010; Martinez-Villalobos & Vimont, 2016, 2017; Vimont, 2010; Wu et al., 2009; H. Zhang et al., 2014). What causes such a season-dependent feature is unknown. Motivated by this observed phenomenon, we intend to construct a theoretical framework to investigate the dependence of the growth rate of the PMM-like perturbation on the mean state. We hypothesize that the man state difference in the surface wind field between boreal spring and other seasons is critical in generating such a season-dependent coupled instability.

The remaining part of this paper is organized as follows. In section 2, using the observed data, we demonstrate the role of the boreal spring mean surface wind in generating the strongest WES feedback through the analysis of wind-induced surface latent heat flux anomalies. In section 3, we examine the growth of a PMM-like perturbation in a simple coupled air-sea model in the presence of boreal spring and fall mean conditions. A conclusion is given in the last section.

2 Phase locking of PMM and estimate of wind induced latent heat flux anomaly

An Empirical Orthogonal Function (EOF) analysis of the SSTA field in the tropical Pacific (20°S-30°N, 150°E-85°W) was first caried out to reveal the spatial patterns and time evolution of the two leading modes. The datasets used in the current study include (1) monthly SST data from the Hadley Centre Global Sea Ice and Sea Surface Temperature (Rayner, 2003) and (2) monthly 10m wind, monthly 850hPa wind and monthly precipitation data from the ERA5 global reanalysis (Hersbach et al. 2020). All the data above are interpolated to 1°×1° grid points using linear interpolation. Monthly climatological fields from 1980 to 2018 are subtracted to obtain the anomalies.

As expected, the first EOF mode shows a pronounced ENSO structure, with the largest SSTA in the equatorial eastern Pacific (Fig. 1a). It explains 53.4% of total variance. The second mode exhibits a PMM-like structure, with a maximum SSTA elongated from northeastern tropical Pacific to equatorial western Pacific (Fig. 1b). It explains 13.2% of total variance. Associated anomalous wind fields were derived by regressing the wind field onto the principal components (PCs) of the first two EOF modes (shown in Fig. 1c).

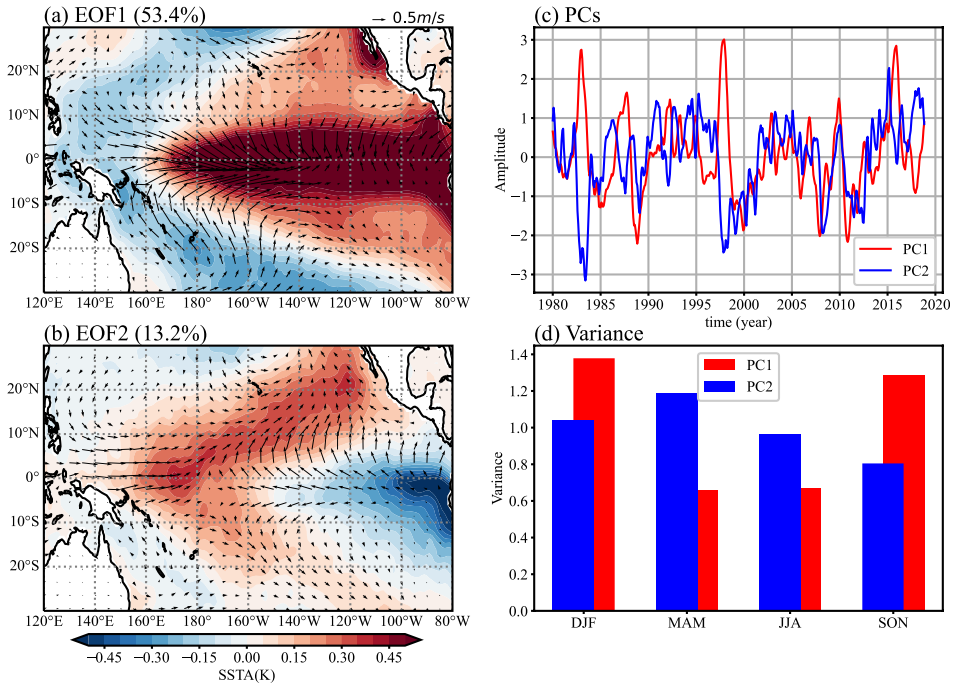

Fig. 1 The result of the EOF method. The first and second EOF patterns **(a-b)** of the SSTA (shaded, unit: °C) in the tropical Pacific (20°S-30°N, 150°E-85°W) during 1980-2018. Vectors are 10m wind anomaly fields regressed onto PC1 and PC2. **(c)** Normalized PC1 and PC2. **(d)** Variance of the two leading EOF modes as a function of season.

Another way to obtain the leading patterns is through the Maximum Covariance Analysis (MCA) of both the anomalous SST and wind fields (Bretherton et al. 1992; Chiang and Vimont 2004). The result is quite similar. In fact, the correlation coefficient between the PCs of the EOF modes and the expansion coefficients (ECs) of the MCA modes is about 0.98.

Fig. 1d shows the variance of the two leading modes at each season. While the ENSO mode is strongest in boreal winter (DJF), the PMM retains the greatest strength in boreal spring (MAM) and is weakest in boreal autumn (SON). It has been shown that the ENSO phase locking is likely attributed to a season-dependent coupled instability (Li 1997a; Li and Hsu 2017; Chen and Jin 2020) and the forcing of easterly anomalies in boreal winter over the equatorial western Pacific associated with the development of a Philippine-Sea anomalous anticyclone (Wang et al., 2000, 2003). To reveal the role of the mean state in causing the phase locking of the PMM, we first estimate the wind-induced surface latent heat flux anomaly in two extreme seasons, boreal spring and autumn, using the observational data.

Following Li (1997b), the surface latent heat flux (LHF) anomaly can be written as

$$Q'_{LH} = Q_{LH} - \overline{Q_{LH}} = -\rho_a C_D L_c \left[\left| \mathbf{V}'_s + \overline{\mathbf{V}_s} \right| \left(q_s - q_a \right) - \left| \overline{\mathbf{V}_s} \right| \left(\bar{q}_s - \bar{q}_a \right) \right] \quad (1)$$

where $\rho_a = 1.2 kg \cdot m^{-3}$ is the surface air density, $C_D = 1.4 \times 10^{-3}$ is the drag coefficient, $\mathbf{V_s} = (u_s, v_s)$ represents horizontal surface wind speed at 10m, $L_c = 2.5 \times 10^6 \ \mathrm{J \cdot kg^{-1}}$ is vaporization latent heat per unit mass, $q_s(T_s)$ is the saturation specific humidity at SST T_s, q_0 is air specific humidity at 10m, $\overline{\mathbf{V}_s}$ stands for basic-state surface wind field, and $\mathbf{V}'_s$ represents surface wind anomaly field. A minus sign in the buck formula above indicates that a positive LHF anomaly value increases the SSTA. An empirical relation is used to calculate q_0 based on SST (Li & Wang, 1994)

$$q_0 = 10^{-3} \left(0.972 T_s - 8.92 \right), \quad (2)$$

To obtain the sole effect of the wind anomaly, one may ignore the difference between $q_s - q_a$ and $\bar{q}_s - \bar{q}_a$. To the first order with use of Taylor expansion, one may derive the following equation:

$$Q'_{LH} \approx -\rho_a C_D L_c \left(\bar{q}_s - \bar{q}_a\right) \frac{\mathbf{V}'_s \cdot \bar{\mathbf{V}}_s}{\left|\bar{\mathbf{V}}_s\right|} \tag{3}$$

Because term $\bar{q}_s - \bar{q}_a$ is always positive, an angle between the background wind and the anomalous wind vector being greater than 90 degrees implies a positive LHF anomaly or a heating effect on the local SST. Therefore, the most efficient way for the heating is when the anomalous wind vector is against the mean wind vector.

A key question to be addressed here is that given the same perturbation wind anomaly as shown in Fig. 1b, would the mean-state condition in MAM give rise to a greater LHF anomaly than in SON? The upper panel of Fig. 2 illustrates the so-calculated latent heat flux anomaly fields. To avoid singularity due to vanished mean wind speed, we imposed a low limit for the mean wind speed in Eq. (3), that is, $|\overline{\mathbf{V}_s}| = 1.5\text{m/s}$, if $|\overline{\mathbf{V}_s}| < 1.5\text{m/s}$.

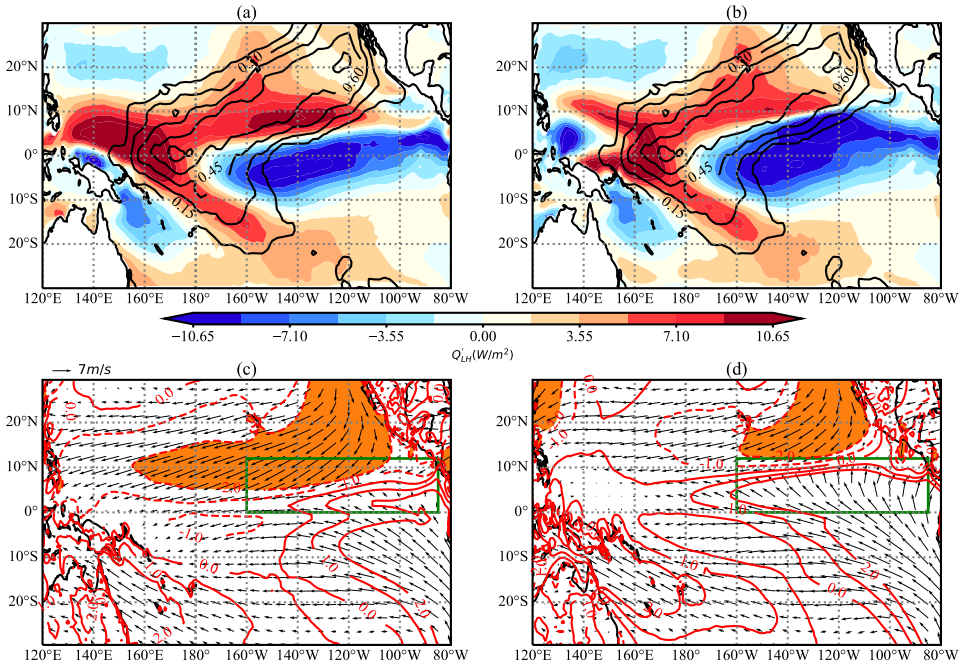

Fig. 2 Wind introduced LHF anomaly and mean Wind field in MAM and SON. **(Upper)** Wind induced LHF anomaly (shaded, Wm^{-2}) fields in MAM (a) and SON (b) calculated based on Eq. 3. The same perturbation

wind derived from Fig. 1b is used. Superposed is the PMM SSTA pattern (contour) shown in Fig. 1b. **(Bottom)** Climatological mean 10m wind fields (vector) in MAM (c) and SON (d). Contour shows the mean meridional wind field at 10m. Orange shading denotes the region where the mean northerly speed exceeds 2 ms^{-1} in the northeasterly trade zone. The green box denotes a contrasting region between pronounced northward cross-equatorial flow in SON and southward retreat of the cross-equatorial flow in MAM.

It can be clearly seen that the difference between the LHF anomalies in MAM and SON lies mainly in the tropical central-eastern Pacific over the PMM region. A greater LHF anomaly occurs in MAM, which may lead to a stronger heating to warm the SSTA over the PMM region. Given the same perturbation wind field, this difference is purely caused by the mean state conditions between MAM and SON. A further separation of effects of the mean wind and SST fields shows that the LHF difference is primarily caused by the wind field (figure not shown).

The aforementioned mean wind effect may be easily seen by pronounced Trade Wind Region (TWR, denoted by shaded area in the bottom panel of Fig. 2). In MAM, the equatorial cold tongue is weakest (Li & Philander, 1996), which leads to the southernmost location for the ITCZ. As a result, strong northeasterly trade winds cover the most of tropical North Pacific. This allows most efficient WES feedback north of the equator. In contrast, the equatorial cold tongue is strongest in SON, and as a result, the ITCZ shifts northward and TWR covers a much smaller area. This leads to a less efficient WES feedback.

The observational analysis above indicates that the mean-state wind in MAM favors a stronger LHF heating and thus a greater development potential for the PMM. In the subsequent section we will further test this hypothesis with a coupled atmosphere-ocean model.

3 Growth rates of PMM-like perturbation in a simple coupled model

A Cane-Zebiak type of coupled atmosphere-ocean model (Zebiak & Cane, 1987) is used. The atmospheric component is the first-baroclinic mode free-atmosphere model (Gill, 1980), with the heating anomaly depending on the perturbation and mean SST. The governing equations of the model are as follows:

$$\varepsilon \mathbf{V}_s' + \beta y \mathbf{k} \times \mathbf{V}_s' = -\frac{1}{\rho_a} \nabla p' \tag{4}$$

$$\varepsilon_p p' + c_0^2 (\nabla \cdot \mathbf{V}_s') = -(\alpha T) \exp((\bar{T} - 30°C)/16.7°C) \tag{5}$$

where ε and ε_p are constant Rayleigh friction and Newtonian damping coefficient, c_0 denotes the first baroclinic mode gravity wave speed, T' and $\bar{T}$ denote anomalous and mean SST. The atmospheric model simulates the anomalous surface wind response to a SSTA in the presence of a specified background mean SST.

The oceanic component includes reduced gravity oceanic dynamics that describe the ocean thermocline (h) and upper-ocean current ($\mathbf{v}$) changes and a momentum equation that describes current shear ($\tilde{\mathbf{v}}$) between the mixed layer and the layer below (Zebiak and Cane 1987). In addition, a mixed-layer temperature (T) equation is utilized to predict the SSTA change due to 3-dimensional temperature advection and surface latent heat flux anomalies. The governing equations of the oceanic component may be written as:

$$\frac{\partial \mathbf{v}}{\partial t} + f\mathbf{k} \times \mathbf{v} = -g' \nabla h + \frac{\boldsymbol{\tau}}{\rho H} - r\mathbf{v} + \nu \nabla^2 \mathbf{v} \tag{6}$$

$$\frac{\partial h}{\partial t} + H \nabla \cdot \mathbf{v} = -rh + \kappa \nabla^2 h \tag{7}$$

$$f\mathbf{k}\times\tilde{\mathbf{v}}=\frac{\boldsymbol{\tau}}{\rho H_1}-r_s\tilde{\mathbf{v}} \tag{8}$$

$$\frac{\partial T}{\partial t}+\mathbf{v}_1\cdot\nabla(\bar{T}+T)+\overline{\mathbf{v}_1}\cdot\nabla T=-[M(\bar{w}+w)-M(\bar{w})]\bar{T}_z$$
$$-M(\bar{w}+w)T_z+\frac{Q}{\rho C_w H_1}-\alpha T+\kappa\nabla^2 T \tag{9}$$

$$\mathbf{v}_1=\mathbf{v}+\frac{H_2}{H}\tilde{\mathbf{v}} \tag{10}$$

where $\mathbf{v}_1$ denotes mixed-layer current, and w is vertical velocity at the base of the mixed layer determined by the divergence of the mixed-layer current. All dependent variables with (without) an overbar denote the mean (anomaly) field. For details about the simple couped model, the readers are referred to Li and Philander (1996) and Li (1997b).

The background mean state fields are specified from the GODAS ocean reanalysis datasets (Xue et al., 2017). For each numerical experiment, the coupled model was integrated for 60 days. Initially a SSTA pattern resembling the observed PMM shown in Fig. 1b with an amplitude of 0.5°C is specified.

To focus on the perturbation development in the off-equatorial region, we intentionally suppress the ENSO mode by applying a strong thermal damping (with a revised time scale of 60 days) in the equatorial zone (4°N and 4°S). Fig. 3a shows the latitudinal distribution of this thermal damping. It is a constant in the equatorial zone, and decreases linearly to zero at 10°N and 10°S.

Two control experiments, CTL_ MAM and CTL_SON, are designed to investigate the growth of the initial PMM pattern under the MAM and SON mean conditions. In the former (latter), the background mean wind and SST fields in MAM (SON) are specified (Table 1). The numerical model results show that the perturbation grows under both the MAM and SON mean conditions,

while keeping its pattern little changed. This implies that the PMM is an unstable mode in both boreal spring and fall.

Table 1 List of numerical experiments with specified background state

Experiment Name	Surface wind background field	SST background field
CTL_MAM	MAM	MAM
CTL_SON	SON	SON
SEN_MAM	MAM	SON
SEN_SON	SON	MAM
SEN_Mix	Mix#	SON

Mix means that the mean wind field in SON is used everywhere except in the region (160°W-85°W, 0°-12°N) where the MAM mean wind is used.

Figs. 3c and d show the simulated anomalous SST and surface wind patterns averaged during the initial 30 days. Both the SST and wind fields are normalized first before a time average is performed. As seen from Fig. 3c and d, the most unstable mode in the region has a northeast-southwest tilted SSTA pattern similar to the PMM in both CTL_MAM and CTL_SON.

While the normalized fields are used to represent the true pattern of the unstable mode, the amplitude of the PMM perturbation may be measured through an area averaged SSTA index over the green quadrilateral domain shown in in Fig. 3c, d. This domain covers the main PMM activity region, with four vertices at (164°W, 7°N), (145°W, 7°N), (110°W, 17°N) and (120°W, 22°S)

194 respectively. Fig. 3b illustrates the time evolutions of the domain-averaged PMM intensity index
195 in the two control experiments. They show an exponential growth characteristic during initil 30
196 days.

197 The growth rate may be estimated from the time evolution curves, say, from day 5 to day 30.
198 Table 2 shows the calculation result for all experiments. Note that the PMM in CTL_MAM grows
199 at a much faster rate than in CTL_SON. Additional parallel experiments with the northern winter
200 (DJF) and summer (JJA) mean conditions were carried out, and the result indicates that their
201 growth rates are somewhere between CTL_MAM and CTL_SON. Therefore, the simple coupled
202 model experiments demonstrate that the PMM is most pronounced in boreal spring, which agrees
203 well with the observations.

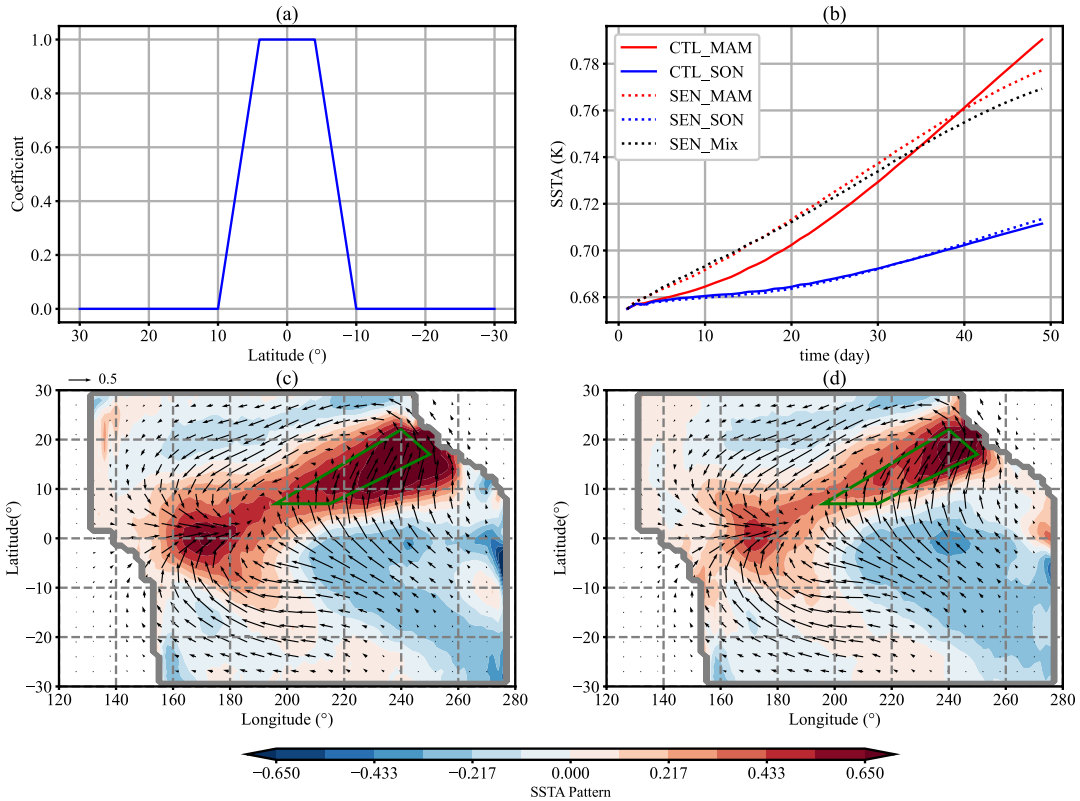

Fig. 3 The damping coefficients, pattern and strength of the experiments. **(a)** The meridional distribution of a thermal damping coefficient in the SSTA equation. with latitude. **(b)** Evolutions of the PMM intensity

index in CTL_MAM (solid red), CTL_SON (solid blue), SEN_MAM (dashed red), SEN_SON (dashed blue) and SEN_Mix (dashed black). **(c)-(d)** The anomalous SST and wind patterns of the most unstable mode in the simple coupled model, averaged during the first 30 days, in CTL_MAM (c) and CTL_SON (d). The green quadrilateral box is used to calculate the PMM strength index.

Table 2 Estimated growth rates at different experiments

Experiment Name	Growth Rate (1/year)
CTL_MAM	1.05
CTL_SON	0.28
SEN_MAM	1.13
SEN_SON	0.28
SEN_Mix	1.02

Two sensitivity experiments were carried out to reveal the relative importance of the background mean wind and SST fields. In SEN_MAM, we keep the same mean wind field as in CTL_MAM but use the SON mean SST condition. In SEN_SON, we keep the same mean wind field as in CTL_SON but use the MAM mean SST condition. Dashed red and blue curves in Fig. 3b represent the evolutions of the PMM intensity in the two sensitivity experiments. Note that the dashed curves are close to the solid ones, suggesting that the coupled instability associated with the PMM is primarily attributed to the mean wind field, while the mean SST plays a minor role.

To reveal the role of the trade wind area in the PMM development, we conducted an additional sensitivity experiment, SEN_Mix. As seen from Fig. 2c, d, the largest difference between the MAM and SON mean wind fields appears in the green box (160°W-85°W, 0°-12°N) in Fig. 2c, d. In SON, this box is dominated by northward cross-equatorial winds, while in MAM, northeasterly trade winds occupy a half of the region. To examine how important the mean wind difference in the region is, we designed this additional experiment (SEN_Mix) in which all mean state conditions are same as CTL_SON except that the mean wind in the box is replaced by its MAM counterpart. A black dashed curve in Fig. 3b represents the time evolution of the simulated PMM intensity in this case. The growth rate in this experiment is much greater than that in CTL_SON (Table 2), and its value is closer to that in CTL_MAM. Thus, this additional sensitivity experiment reveals the critical role of the mean trade wind area, in particular, southward penetration of the northeasterly trade, in promoting a stronger PMM development through the WES feedback.

4 Conclusion

Why the PMM is most pronounced in boreal spring is investigated through a combined observational and modeling study. In the observational analysis, we compare wind-induced LHF anomaly fields in the presence of MAM and SON mean conditions. It is found that even given the same PMM related perturbation wind field, the strongest heating effect on SST occurs in MAM. The cause of the season-dependent feature lies on the strength and area of the background northeasterly trade north of the equator. In MAM, the equatorial cold tongue is weakest and the ITCZ is at southernmost location. As a consequence, the northeasterly trade covers almost entire tropical North Pacific. This allows most active WES feedback in the region. It is opposite in SON, when the ITCZ is at northernmost location and the northeasterly trade area is greatly shrunk.

Therefore, the preferred development of the PMM in MAM is attributed to the greatest strength and largest area of the northeasterly trade.

A simple coupled atmosphere-ocean model is further used to test the mean state control hypothesis. It is an anomaly coupled model in which a seasonal mean state is specified. Two control experiments are designed, in which the background mean wind and SST fields are specified from the MAM and SON conditions. Initially a PMM like SSTA pattern with a moderate amplitude is specified. The numerical experiments demonstrate that the PMM is most unstable mode in the off-equatorial region and that the strongest growth of the PMM perturbation occurs in MAM. Further sensitivity experiments are designed to reveal the relative importance of the mean wind and SST fields in promoting the PMM development. It is found that the instability lies primarily on the mean wind field. It is the greatest strength and area of the mean northeasterly trade that allows most efficient wind-evaporation-SST feedback and thus the PMM development in MAM.

It is worth mentioning that while the advantage of use of a simple model is the specification of a fixed mean state and the inclusion of only essential processes, the coupled model involves various assumptions. Among them are the dependence of atmospheric heating on the SSTA and the exclusion of the cloud-radiation-SST feedback and sensible heat fluxes. A further study with use of a coupled atmosphere-ocean general circulation model is needed to test the mean wind control hypothesis and to confirm the simple model results.

Acknowledgments

This work was supported by NSFC grant 42088101 and NSF grant AGS-2006553. This is SOEST contribution number 12345 and IPRC contribution number 1234.

Data Availability Statement

The Hadley Centre Sea Ice and Sea Surface Temperature data sets are publicly available at: https://www.metoffice.gov.uk/hadobs/hadisst/ . And the ERA5 global reanalysis data sets are publicly available at: https://www.ecmwf.int/en/forecasts/datasets/reanalysis-datasets/era5 .

References

Alexander, M. A., Vimont, D. J., Chang, P., & Scott, J. D. (2010). The Impact of Extratropical Atmospheric Variability on ENSO: Testing the Seasonal Footprinting Mechanism Using Coupled Model Experiments. *Journal of Climate*, *23*(11), 2885–2901. https://doi.org/10.1175/2010JCLI3205.1

Amaya, D. J. (2019). The Pacific Meridional Mode and ENSO: a Review. *Current Climate Change Reports*, *5*(4), 296–307. https://doi.org/10.1007/s40641-019-00142-x

Amaya, D. J., Kosaka, Y., Zhou, W., Zhang, Y., Xie, S.-P., & Miller, A. J. (2019). The North Pacific Pacemaker Effect on Historical ENSO and Its Mechanisms. *Journal of Climate*, *32*(22), 7643–7661. https://doi.org/10.1175/JCLI-D-19-0040.1

An, S.-I., & Wang, B. (2001). Mechanisms of Locking of the El Niño and La Niña Mature Phases to Boreal Winter. *Journal of Climate*, *14*(9), 2164–2176. https://doi.org/10.1175/1520-0442(2001)014<2164:MOLOTE>2.0.CO;2

Bretherton, C. S., Smith, C., & Wallace, J. M. (1992). An Intercomparison of Methods for Finding Coupled Patterns in Climate Data. *Journal of Climate*, *5*(6), 541–560. https://doi.org/10.1175/1520-0442(1992)005<0541:AIOMFF>2.0.CO;2

Chen, H.-C., & Jin, F.-F. (2020). Fundamental Behavior of ENSO Phase Locking. *Journal of Climate*, *33*(5), 1953–1968. https://doi.org/10.1175/JCLI-D-19-0264.1

Chiang, J. C. H., & Vimont, D. J. (2004). Analogous Pacific and Atlantic Meridional Modes of Tropical Atmosphere–Ocean Variability. *Journal of Climate*, *17*(21), 4143–4158. https://doi.org/10.1175/JCLI4953.1

Gill, A. E. (1980). Some simple solutions for heat-induced tropical circulation. *Quarterly Journal of the Royal Meteorological Society*, *106*(449), 447–462. https://doi.org/10.1002/qj.49710644905

Hersbach, H., Bell, B., Berrisford, P., Hirahara, S., Horányi, A., Muñoz-Sabater, J., et al. (2020). The ERA5 global reanalysis. *Quarterly Journal of the Royal Meteorological Society*, *146*(730), 1999–2049. https://doi.org/10.1002/qj.3803

Li, T. (1997a). Air–Sea Interactions of Relevance to the ITCZ: Analysis of Coupled Instabilities and Experiments in a Hybrid Coupled GCM. *Journal of the Atmospheric Sciences*, *54*(1), 134–147. https://doi.org/10.1175/1520-0469(1997)054<0134:ASIORT>2.0.CO;2

Li, T. (1997b). Phase Transition of the El Niño–Southern Oscillation: A Stationary SST Mode. *Journal of the Atmospheric Sciences*, *54*(24), 2872–2887. https://doi.org/10.1175/1520-0469(1997)054<2872:PTOTEN>2.0.CO;2

Li, T., & Philander, S. G. H. (1996). On the Annual Cycle of the Eastern Equatorial Pacific. *Journal of Climate*, *9*(12), 2986–2998. https://doi.org/10.1175/1520-0442(1996)009<2986:OTACOT>2.0.CO;2

Li, T., & Wang, B. (1994). A Thermodynamic Equilibrium Climate Model for Monthly Mean Surface Winds and Precipitation over the Tropical Pacific. *Journal of the Atmospheric Sciences*, *51*(11), 1372–1385. https://doi.org/10.1175/1520-0469(1994)051<1372:ATECMF>2.0.CO;2

Lorenzo, E. D., Liguori, G., Schneider, N., Furtado, J. C., Anderson, B. T., & Alexander, M. A. (2015). ENSO and meridional modes: A null hypothesis for Pacific climate variability. *Geophysical Research Letters*, *42*(21), 9440–9448. https://doi.org/10.1002/2015GL066281

Martinez-Villalobos, C., & Vimont, D. J. (2016). The Role of the Mean State in Meridional Mode Structure and Growth. *Journal of Climate*, *29*(10), 3907–3921. https://doi.org/10.1175/JCLI-D-15-0542.1

Martinez-Villalobos, C., & Vimont, D. J. (2017). An Analytical Framework for Understanding Tropical Meridional Modes. *Journal of Climate*, *30*(9), 3303–3323. https://doi.org/10.1175/JCLI-D-16-0450.1

Neelin, J. D., Jin, F.-F., & Syu, H.-H. (2000). Variations in ENSO Phase Locking*. *Journal of Climate*, *13*(14), 2570–2590. https://doi.org/10.1175/1520-0442(2000)013<2570:VIEPL>2.0.CO;2

Rayner, N. A. (2003). Global analyses of sea surface temperature, sea ice, and night marine air temperature since the late nineteenth century. *Journal of Geophysical Research*, *108*(D14), 4407. https://doi.org/10.1029/2002JD002670

Stuecker, M. F. (2018). Revisiting the Pacific Meridional Mode. *Scientific Reports*, *8*(1), 1–9. https://doi.org/10.1038/s41598-018-21537-0

Vimont, D. J. (2010). Transient Growth of Thermodynamically Coupled Variations in the Tropics under an Equatorially Symmetric Mean State*. *Journal of Climate*, *23*(21), 5771–5789. https://doi.org/10.1175/2010JCLI3532.1

Vimont, D. J., Wallace, J. M., & Battisti, D. S. (2003). The Seasonal Footprinting Mechanism in the Pacific: Implications for ENSO. *JOURNAL OF CLIMATE*, *16*, 8.

Vimont, D. J., Alexander, M., & Fontaine, A. (2009). Midlatitude Excitation of Tropical Variability in the Pacific: The Role of Thermodynamic Coupling and Seasonality*. *Journal of Climate*, *22*(3), 518–534. https://doi.org/10.1175/2008JCLI2220.1

Wang, B., Wu, R., & Fu, X. (2000). Pacific–East Asian Teleconnection: How Does ENSO Affect East Asian Climate? *Journal of Climate*, *13*(9), 1517–1536. https://doi.org/10.1175/1520-0442(2000)013<1517:PEATHD>2.0.CO;2

Wang, B., Wu, R., & Li, T. (2003). Atmosphere–Warm Ocean Interaction and Its Impacts on Asian–Australian Monsoon Variation*. *Journal of Climate*, *16*(8), 1195–1211. https://doi.org/10.1175/1520-0442(2003)16<1195:AOIAII>2.0.CO;2

Wu, S., Wu, L., Liu, Q., & Xie, S.-P. (2009). Development processes of the Tropical Pacific Meridional Mode. *Advances in Atmospheric Sciences*, *27*(1), 95. https://doi.org/10.1007/s00376-009-8067-x

Xie, S.-P., & Philander, S. G. H. (1994). A coupled ocean-atmosphere model of relevance to the ITCZ in the eastern Pacific. *Tellus A: Dynamic Meteorology and Oceanography*, *46*(4), 340–350. https://doi.org/10.3402/tellusa.v46i4.15484

Xue, Y., Wen, C., Yang, X., Behringer, D., Kumar, A., Vecchi, G., et al. (2017). Evaluation of tropical Pacific observing systems using NCEP and GFDL ocean data assimilation systems. *Climate Dynamics*, *49*(3), 843–868. https://doi.org/10.1007/s00382-015-2743-6

Zebiak, S. E., & Cane, M. A. (1987). A Model El Ni&ntilde–Southern Oscillation. *Monthly Weather Review*, *115*(10), 2262–2278. https://doi.org/10.1175/1520-0493(1987)115<2262:AMENO>2.0.CO;2

Zhang, H., Deser, C., Clement, A., & Tomas, R. (2014). Equatorial signatures of the Pacific Meridional Modes: Dependence on mean climate state: Zhang et al.: Role of mean state in PMMs' asymmetry. *Geophysical Research Letters*, *41*(2), 568–574. https://doi.org/10.1002/2013GL058842

Zhang, L., Chang, P., & Tippett, M. K. (2009). Linking the Pacific Meridional Mode to ENSO: Utilization of a Noise Filter. *Journal of Climate*, *22*(4), 905–922. https://doi.org/10.1175/2008JCLI2474.1